Pergamon

Int. J. Heat Mass Transfer. Vol. 40, No. 4, pp. 843–856, 1997
Copyright © 1996 Elsevier Science Ltd
Printed in Great Britain. All rights reserved
0017 9310/97 $17.00 + 0.00

PII: S0017-9310(96)00165-2

Simulation of the transport processes in the neck-down region of a furnace drawn optical fiber

S. H.-K. LEE

Department of Mechanical Engineering, The Hong Kong University of Science and Technology, Clear Water Bay, Kowloon, Hong Kong

and

Y. JALURIA

Department of Mechanical and Aerospace Engineering, Rutgers, The State University of New Jersey, New Brunswick, NJ 08855, U.S.A.

(*Received* 12 *December* 1995 *and in final form* 23 *April* 1996)

Abstract—The heating, drawing and cooling of fused silica have a great impact on the overall quality of the fiber. Thus, a clear understanding of the underlying physics is crucial. The present study seeks to evaluate the impact of simplifying assumptions in the treatment of the transport equations and the thermal conditions, as well as to evaluate the feasibility of adapting simpler models. The results showed a localization of the vorticity and viscous dissipation, and confirmed the existence of temperature and velocity gradients. The results also showed the necking shape, heat transfer coefficient and furnace temperature profiles to have a decisive impact on the overall solution. In addition, the approximation of setting the vorticity to zero was found to be a feasible alternative. Copyright © 1996 Elsevier Science Ltd.

1. INTRODUCTION

Optical fibers are the communication media of choice. However, like many other materials processing techniques, this production process is still very much an empirical one. Consequently, technicians usually spend an enormous amount of time, effort and materials in determining the new set of operating conditions for a new fiber or preform. Even then it is not uncommon for fibers, drawn from the same batch of preforms and under the same apparent conditions, to optically differ from one day to another. Clearly, this empirical approach will become insufficient as the growing information superhighway further pushes the demand for fibers of higher quality to cost ratio. The basic problem is the lack of scientific understanding of the inherent transport processes and their effects on the fiber quality. As discussed later, much of this is due to the complexity of the inherent transport processes.

Fiber characteristics such as optical loss, optical dispersion, communication bandwidth and static/fatigue strength are all directly or indirectly affected by the transport processes during the production [1] as well as by the residual stress and the dimensional irregularities of the fiber [2]. Figure 1 shows a schematic of the production process which can be separated into three distinct regions: the neck-down region is where the fused silica rod (preform) is heated and drawn into a fiber, while the cooling region is where the fiber cools to the requisite temperature before entering the final coating region for protection. Our present focus is on the transport at the neck-down region, as shown in Fig. 2.

To study this transport is not a trivial task. In general, not only is the transport a complex coupling between conduction, convection and radiation, but one of the radiative surfaces is also spectral. In addition, this problem embodies dramatic gradients stemming from both the large changes in the preform diameter, from 1.2 cm to 120 μm, and its viscosity, from approximately 13 million to 21 $m^2 s^{-1}$. Further compounding the difficulty of this problem is the lack of data. The thermal/physical properties of fused silica are largely unknown, and indeed, many researchers still refer to 30 year old data compiled by Fleming [3]. In addition, the temperature distribution in the furnace, the nature of the convective heat transfer and the shape of the preform (necking shape) are also unknown.

In the past 20 years there has in fact been some work done in this area [4]. In general much of this, including a lot from Russian researchers, was of limited value since the assumptions were often inconsistent and sometimes unacceptable. The studies by Paek and Runk [5], Sayles [6] and Myers [7] were

NOMENCLATURE

a	absorption coefficient
e	black body emissive power
F	view factor
h	heat transfer coefficient
L	length of furnace
N	number of radiative sections
n	index of refraction
n, t	outward normal and tangential unit vectors
q	radiative flux [W m^{-2}]
qe	equivalent heat flux, $(\sigma/L)\int T_f(z)^4\,dz$
Q	radiative power [W]
R	radius
$S_{k\,j}$	distance from kth segment to jth segment
S_v	source term due to variable viscosity
T^*	temperature, T/T_m
t^*	time, t/R_i
u^*, v^*	radial and axial velocity, u/v_i and v/v_i.

Greek letters

ε	hemispherical emissivity
η, β	transformed coordinates, r/R and z/L
θ	viewing angle
λ	wavelength
λb, λi, λo	black body, incoming and outgoing (spectral)
μ, ν	dynamic and kinematic viscosity
ξ	surface tension
σ	Stefan–Boltzman constant
Φ	viscous dissipation
ψ, Ψ	streamfunction, $\Psi = \psi/R_i^2 v_i$
ω, Ω	vorticity, $\Omega = \omega R_i/v_i$.

Subscripts

1, 2	location where necking begins and ends
c, s	center and surface value
f	furnace value
i, e	inlet and exit value
m	softening point of fused silica, taken to be 1900 K
∞	ambient temperature, 1373 K.

among those which were markedly better than the others in rigor and sophistication, although even these required substantial improvements. In general, they assumed that the radiative exchange existed only between the furnace and the preform surfaces; that is, it was not treated as an enclosure exchange as it should have been. Also, except for Myers [7], all have ignored the spectral dependence of the fused silica. In addition, most researchers performed only 1-D analyses. Those performing 2-D analyses assumed only a one order of magnitude reduction in diameter and/or a weaker viscosity dependence that varied with $1/T$ as opposed to $\exp(1/T)$. Almost none have performed a 2-D analysis coupled with both a two orders of magnitude reduction in diameter and a viscosity dependence of $\exp(1/T)$, since such an analysis presents serious convergence difficulties as readily acknowledged by Sayles [6]. Furthermore, almost everyone ignored the presence of viscous dissipation. The one exception was Sayles [6] who unfortunately used the weaker viscosity dependence of $1/T$. Finally, everyone used either an analytically or experimentally inferred furnace temperature distribution, but none have attempted to determine the impact of an error in such an inference.

Clearly, the motivation for this work is to obtain a computer model of the transport, so that it could later be coupled with an appropriate materials study and be used to predict and improve fiber qualities. However, as mentioned earlier, there are many difficulties involved. Thus, besides developing the computationally efficient algorithms to address the large gradients as well as the large dimensional and property changes, the impact of many of the unknowns needs to be systematically determined. Therefore, several questions need to be considered, the answers to which will dictate the requisite sophistication and complexity of the computer model as well as clarifying areas requiring immediate attention. For example, is the radiative exchange between only two surfaces sufficient? Of the many properties that are variable, which ones can be ignored? Is the inclusion of viscous dissipation necessary? Is a 2-D analysis necessary, or will a 1-D analysis be sufficient? Since the profiles of heat transfer coefficient, necking shape and furnace temperature may be unknown, what impact does each have on the overall solution? Some of these have been answered by Lee and Jaluria in previous studies. Thus, the algorithms for the large gradients and dimensional changes have been developed in the course of a study on the laminar forced convection within axisymmetric ducts [8]. In a later work, Lee and Jaluria [9] studied the radiative exchange between two stationary and concentric cylindrical bodies, and showed that an enclosure analysis is required since the heat flux absorbed by the preform at the neck-down region is affected by the self-viewing of the furnace. Finally, in a more recent work, Lee and Jaluria [10] studied the free surface flow of silica subjected to a fixed heat flux, and showed that the most crucial data is the viscosity dependence on temperature and that furthermore 2-D analyses are necessary as the viscous dissipation had considerable impact on the local temperature.

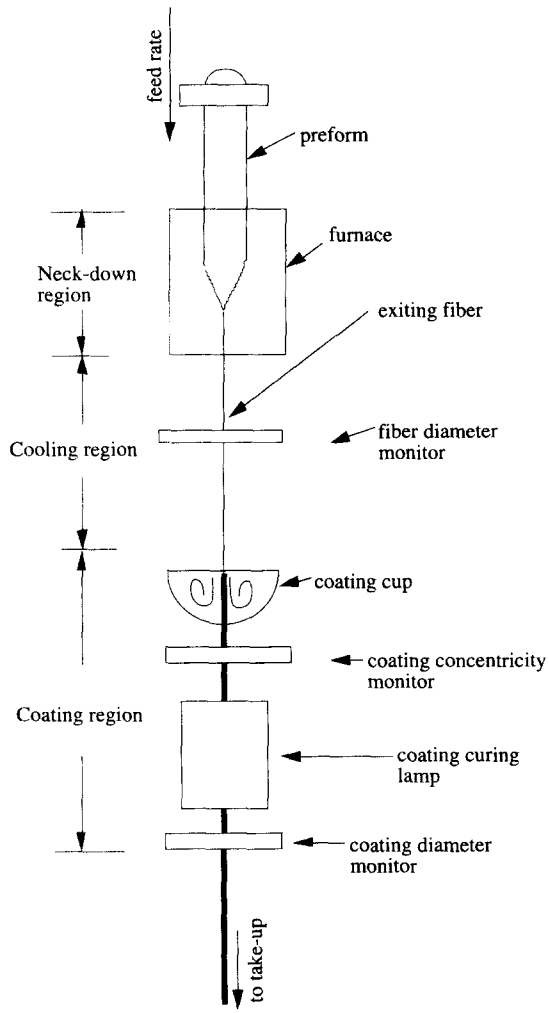

Fig. 1. Schematic showing the different regions of interest during the drawing of optical fibers.

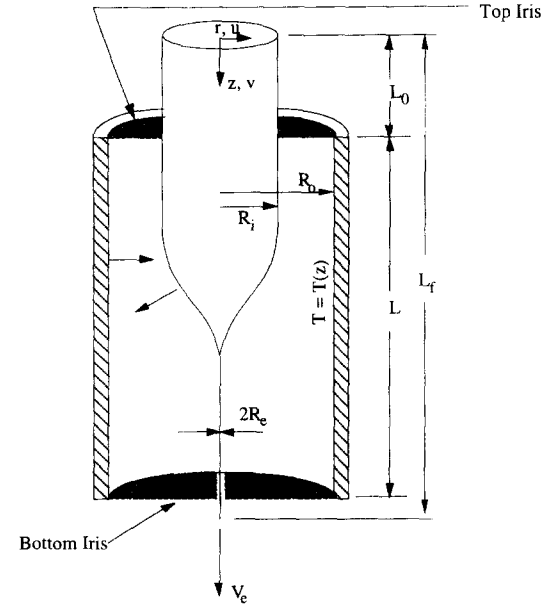

Fig. 2. Schematic of the neck-down region within the furnace and the geometrical configuration.

The present work is the substantive sum of all the previous studies by Lee and Jaluria [8–10]. Thus, whereas each of the previous works was aimed at bringing out the physics of independent aspects of the necking region, the present one is the first to combine all the tools and knowledge obtained thus far and addresses some of the larger issues still remaining. One of the objectives is to determine the feasibility of adapting substantially simpler models for situations where approximate simulations are sought. In addition, this study seeks to determine the relative importance of the many unknowns in this problem, so that after they are properly addressed, a more sophisticated model can be developed for prediction under different drawing conditions. As mentioned earlier, many of these have already been determined in our previous studies. What remains is to determine the impact of the necking shape, the furnace temperature distribution and the convective heat exchange. That is, how important is it to arrive at exact expressions for the neck shape and the thermal conditions? As evidenced by the large amount of work using seemingly arbitrary assumptions, the exact expressions indeed require very intensive efforts. However, for situations where only the temperature gradients may be important, it might be possible to use some reasonable estimates instead.

2. ANALYSIS

All the relevant configurations, as shown in Fig. 2, were chosen to be consistent with the data available in the literature and whenever possible cross-checked against one another. This included the neck shape, although it should really be a result of the overall computation and should not be prescribed *a priori*. The neck shape is the result of the local force balance along the free surface, and its computation is beyond the scope of this study. The potential impact of prescribing a neck shape, consistent with measurements [5], is discussed in greater detail in Section 3. The neck shape, the physical geometries and the thermal conditions are given in Appendix A.

The axisymmetric, free-surface flow of fused silica with viscous dissipation was considered, where the thermal and physical properties were taken to be temperature dependent, as discussed in greater detail in Appendix B. The thermal transport within this silica was coupled with the convective and radiative exchange in the enclosure, in which the former was addressed through the use of an axially variable heat transfer coefficient [11]. The radiative transport within the enclosure was modeled as surface exchanges where properties of the furnace and preform were taken to be consistent with those of Myers [7] and Sayles [6]. That is, the furnace was treated as a diffuse gray sur-

face and the preform was treated as a diffuse spectral surface. The preform, consisting of fused silica, is transparent and has relatively low emissivity values. However, available data show that within a narrow bandwidth, it can be approximated with a two-band model [7]. Unfortunately, due to the lack of improved data and the fact that the extinction coefficient is quite high within these bands, an optically thick assumption was used as a first cut approximation for the internal radiation.

2.1. *Governing equations*

The laminar free-surface flow of fused silica with a prescribed necking shape and variable properties was considered. The necking geometry was mapped into a rectangular domain [12], and the time-dependent energy equation as well as the Ψ–Ω equations were transformed and solved on a non-uniform grid [8]. Including the effects of viscous dissipation and variable properties, the energy equation for the fused silica is expressed below in equation (1a) in terms of the transformed coordinates η and β.

$$\frac{\partial T^*}{\partial t^*}+\frac{v_i R_i}{R}\frac{\partial}{\partial \eta}(\eta u^* T^*)+\frac{v_i R_i}{L}\frac{\partial}{\partial \beta}(v^* T^*) -\eta\frac{v_i R_i}{R}\frac{dR}{dz}\frac{\partial}{\partial \eta}(v^* T^*) =\frac{1}{\rho c_p}\left[\frac{R_i}{\eta R^2}\frac{\partial}{\partial \eta}\left(k\eta\frac{\partial T^*}{\partial \eta}\right)+\frac{R_i}{L^2}\frac{\partial}{\partial \beta}\left(k\frac{\partial T^*}{\partial \beta}\right) -\frac{\eta R_i}{L}\frac{\partial}{\partial \beta}\left(\frac{k}{R}\frac{dR}{dz}\frac{\partial T^*}{\partial \eta}\right)-\frac{\eta R_i}{RL}\frac{dR}{dz}\frac{\partial}{\partial \eta}\left(k\frac{\partial T^*}{\partial \beta}\right) +\frac{\eta R_i}{R^2}\left(\frac{dR}{dz}\right)^2\frac{\partial}{\partial \eta}\left(k\eta\frac{\partial T^*}{\partial \eta}\right)\right]+\frac{R_i\Phi}{c_p T_m}. \tag{1a}$$

The last term in equation (1a) represents the viscous dissipation, and is shown below as:

$$\Phi = 2\nu v_i^2\left[\frac{1}{R^2}\left(\frac{\partial u^*}{\partial \eta}\right)^2+\left(\frac{1}{L}\frac{\partial v^*}{\partial \beta}-\frac{\eta}{R}\frac{dR}{dz}\frac{\partial v^*}{\partial \eta}\right)^2 +\left(\frac{u}{\eta R}\right)^2+\frac{1}{2}\left(\frac{1}{L}\frac{\partial u^*}{\partial \beta}-\frac{\eta}{R}\frac{dR}{dz}\frac{\partial u^*}{\partial \eta}+\frac{1}{R}\frac{\partial v^*}{\partial \eta}\right)^2\right]. \tag{1b}$$

Similarly, the streamfunction and vorticity equations are given as:

$$\left(\frac{R_i}{R}\right)^3\frac{\partial}{\partial \eta}\left(\frac{1}{\eta}\frac{\partial \Psi}{\partial \eta}\right)+\left(\frac{R_i}{R}\right)^3\left(\frac{dR}{dz}\right)^2\eta\frac{\partial^2\Psi}{\partial \eta^2} +\left[2\left(\frac{dR}{dz}\right)^2\left(\frac{R_i}{R}\right)^3-\frac{R_i^3}{R^2}\frac{d^2R}{dz^2}\right]\frac{\partial \Psi}{\partial \eta} -\frac{2R_i^3}{R^2L}\frac{dR}{dz}\frac{\partial^2\Psi}{\partial \eta\,\partial \beta}+\frac{R_i^3}{RL^2}\frac{1}{\eta}\frac{\partial^2\Psi}{\partial \beta^2}=-\Omega \tag{2}$$

$$\left(\frac{v_i R_i}{R}\right)\frac{\partial}{\partial \eta}(u^*\Omega)-\frac{dR}{dz}\left(\frac{v_i R_i}{R}\right)\eta\frac{\partial}{\partial \eta}(v^*\Omega) +\left(\frac{v_i R_i}{L}\right)\frac{\partial}{\partial \beta}(v^*\Omega) =\nu\left[\frac{R_i}{R^2}\frac{\partial}{\partial \eta}\left(\frac{1}{\eta}\frac{\partial}{\partial \eta}(\eta\Omega)\right)+\left(\frac{\eta}{R}\right)^2\left(\frac{dR}{dz}\right)^2 \times R_i\frac{\partial^2\Omega}{\partial \eta^2}-\frac{2\eta R_i}{RL}\frac{dR}{dz}\frac{\partial^2\Omega}{\partial \eta\,\partial \beta} -\frac{\eta R_i}{R}\left(\frac{d^2R}{dz^2}-\frac{2}{R}\left(\frac{dR}{dz}\right)^2\right)\frac{\partial \Omega}{\partial \eta}+\frac{R_i}{L^2}\frac{\partial^2\Omega}{\partial \beta^2}\right]+\frac{R_i^2}{\nu_0}S_v. \tag{3a}$$

The last term in equation (3a), S_v, represents the vorticity source term due to variable viscosity and is given in equation (3b) where each term can be expressed in terms of u^*, v^*, and the transformed coordinates, η and β [4].

$$S_v=\frac{\partial v}{\partial z}\left[2\frac{\partial^2 u}{\partial r^2}+2\frac{\partial^2 u}{\partial z^2}+\frac{2}{r}\frac{\partial u}{\partial r}-\frac{2u}{r^2}\right] +\left(\frac{\partial^2 v}{\partial z^2}-\frac{\partial^2 v}{\partial r^2}\right)\left[\frac{\partial u}{\partial z} +\frac{\partial v}{\partial r}\right]+\frac{\partial^2 v}{\partial r\,\partial z}\left[2\frac{\partial u}{\partial r}-2\frac{\partial v}{\partial z}\right]-\frac{\partial v}{\partial r} \times\left[2\frac{\partial^2 v}{\partial r^2}+2\frac{\partial^2 v}{\partial z^2}+\frac{1}{r}\left(\frac{\partial v}{\partial r}+\frac{\partial u}{\partial z}\right)\right]. \tag{3b}$$

Coupled to the energy transport within the silica is the radiative transport between the preform, the furnace and the irises. The corresponding expression for the net energy on a diffuse, spectral surface is given in equation (4) in terms of the difference between the outgoing and incoming energy.

$$Q_k=\int_0^\infty dQ_{\lambda,k}=\int_0^\infty dQ_{\lambda o,k}-\int_0^\infty dQ_{\lambda i,k}. \tag{4}$$

By expressing this incoming energy as the sum of the energy received from the other surfaces, and dividing by the area, equation (4) becomes:

$$q_k=\int_0^\infty dq_{\lambda,k}=\int_0^\infty dq_{\lambda o,k}-\sum_{j=1}^{N}\left(\int_0^\infty dq_{\lambda o,j}\right)F_{k\,j}. \tag{5}$$

In order to solve for the heat flux from equation (5), the individual integrals must be first evaluated by applying the band approximation [9] to the definition of the radiosities, to get:

$$\int_0^\infty dq_{\lambda o,k}=\int_3^8 dq_{\lambda o,k}=\int_3^8\varepsilon_{\lambda,k}e_{\lambda b,k}\,d\lambda +\sum_{j=1}^{N}\left(\int_3^8(1-\varepsilon_{\lambda,k})\,dq_{\lambda o,j}\right)F_{k\,j}. \tag{6}$$

Equation (6) can be readily solved once the spectral properties are determined and the view factors are computed from equation (7) below.

$$F_{k-j} = \frac{1}{A_k}\int\left(\int \frac{\cos\theta_k \cos\theta_j}{\pi S_{k-j}^2}\,\mathrm{d}A_j\right)\mathrm{d}A_k$$

$$= \int \frac{\cos\theta_k \cos\theta_j}{\pi S_{k-j}^2}\,\mathrm{d}A_j. \tag{7}$$

2.2. *Boundary conditions*

At the inlet, the fiber enters with a uniform velocity and loses heat to its surroundings through convection. Dropping the asterisks for convenience, this is given below as:

$$\Psi(\eta : 0.1) = \frac{\eta^2}{2}, \quad \Omega = 0, \quad \frac{\partial T}{\partial \beta} = \frac{hL}{k}(T_{z=0} - T_\infty). \tag{8a}$$

At the end of the necking region, the fiber reaches a uniform velocity, and thus a developed condition was imposed for the streamfunction and vorticity. However, due to the presence of viscous dissipation, the temperature at the exit may not necessarily attain a developed condition. Therefore, a zero diffusion condition was prescribed instead, which is consistent with the large *Pe* number at the exit. Independence of the solution from this assumption was verified by extending the computational domain. These conditions are given below as:

$$\frac{\partial \Psi}{\partial \beta} = \frac{\partial \Omega}{\partial \beta} = \frac{\partial^2 T}{\partial \beta^2} = 0. \tag{8b}$$

Also, recognizing symmetry at the center, the boundary conditions there became:

$$\Psi = 0, \quad \Omega = 0, \quad \frac{\partial T}{\partial \eta} = 0. \tag{8c}$$

Finally, at the interface, there exists a surface tension which may give rise to flows [10, 13]. At the same time, this surface is also subjected to a convective and radiative exchange. These conditions are given below in equation (8d).

$$\Psi = \frac{1}{2}, \quad \Omega = \frac{-R_1}{\mu v_1}\frac{\partial \xi}{\partial \mathbf{t}}, \quad -k\frac{\partial T}{\partial \mathbf{n}} = h(T_s - T_\infty) - q. \tag{8d}$$

Note from this equation, the inverse relation between the vorticity and the local viscosity. Also, the last term in this equation served to couple the energy transport within the silica to the radiative flux from the furnace, which was obtained by solving equations (5)–(7) above.

2.3. *Method of solution*

Using the previously developed transformation technique, the Ψ–Ω equations and the time-dependent energy equation were mapped into a rectangular domain [8]. The transformed equations were then approximated using a custom design non-uniform grid [8], in order to properly capture the large viscosity gradients which are exponentially dependent on the local temperatures. To increase the accuracy, a nominally second-order finite difference scheme was developed [8]. Central differencing was applied to all except the advection terms of the energy equation, which were approximated with a hybrid scheme [14]. The resulting algebraic expressions were underrelaxed and solved using the ADI and the red–black reduction schemes [15]. Recognizing the strong nonlinearity in the system which arises from the coupling between the exponentially variable viscosity and the viscous dissipation [10], a transient energy equation was used to temporally lead the computation in order to ensure proper convergence.

This energy equation was coupled with the radiative exchange through the boundary condition given above in equation (8d). The solution to equations (5)–(7) requires both the radiative properties and computation of the view factors [9]. In general, a band approximation was used on the emissivity, which is consistent with the available data in the literature. The view factor was computed numerically, and there are several features of this configuration which inhibit the use of the many algorithms which are readily available in the literature. The present algorithm [9] does not impose restrictions on the shape of the preform, except that it must be continuous. As such, its shape may be excessively steep or even sinusoidal, as may occur during drawing instabilities. Reciprocity relations are not explicitly enforced, and it allows for the self-viewing of the enclosure and viewing obstructions by the preform. To achieve computational efficiency, a nonuniform grid was developed to reduce errors at the corners, and a bisection search method was implemented. This is particularly important since, in general, each viewing factor consists of four terms, each being a matrix of order 5000×5000.

The solution process began with the assumption of initial temperature and velocity distributions. From this initial temperature, the properties and the radiative heat flux were evaluated. The Ψ–Ω equations were then iterated once for the new velocity, which were then used as the temperature equation marched one time-step. From the new temperatures, the properties and the radiative flux were re-evaluated, and a new velocity distribution was again obtained from a single iteration of the Ψ–Ω equations. This process was repeated until convergence was achieved. The solutions were then verified for independence of user prescribed parameters.

Two convergence criteria were concurrently used. In one, the infinity norm condition was used to ensure that the maximum difference between two successive computations of T, Ψ, and Ω in the entire computational domain reached a constant value [8]. This ensures that a small difference reflects a true steady-

state value, which, depending on the variable, may be around 10^{-10}. In the second criterion, the infinity norm condition was applied to the residuals of the energy, streamfunction and the vorticity equations, so that the computations continued until they reached a constant value, which were generally smaller than 10^{-10}.

3. RESULTS AND DISCUSSION

To evaluate the effect of the neck shape and thermal conditions, solutions were first obtained for a base system, where all the relevant configurations were taken to be consistent with those of an actual experiment, and then compared with results where the neck shape and the thermal conditions were systematically varied. If a particular variation produced no significant changes in the temperature distribution, then it was likely not to have been of first-order importance. As discussed in Appendices A and B, these variations were chosen to be realistic. It should be noted that the prescription of a neck shape may be of concern, as in reality, it is part of the solution and may vary in response to variations in the system. However, for this particular study, this is of a lesser concern since if a particular variation produced significant changes when a neck shape is prescribed, it will also produce changes if the neck shape were allowed to vary.

3.1. *Validation*

Due to the limited amount of similar work in the available literature, validation through direct comparison was difficult. Therefore, the validation efforts of our previous studies [8–10] form the most significant measure of correctness for the present study. In general, these comparisons were made for degenerate cases where results were more readily available [16–25]. In the degenerate case of laminar convection in axisymmetric ducts with streamwise variable radii, the obtained results were nearly identical to those in the literature [21–24] with the singular exception of Garg and Maji's results [21] which did not reach proper convergence. Comparisons for flow with variable viscosity and viscous dissipation were equally encouraging [16–20], where, in almost all cases, the graphs were again nearly identical. In fact, the computed asymptotic Nusselt number of 9.6 was in exact agreement with Lin *et al.* [18]. The only minor discrepancy was with two approximate solutions, but it was most likely due to the latter's neglect of axial diffusion and early truncation of the series solution. Validation was also obtained for the radiative analysis, where the un-enforced reciprocity relations and the sum of the computed view factors, for varying necking shapes, were consistent with expectations. Also, the analytical view factors for the degenerate cases matched the computed values to within 0.2%. In addition, the radiative energy transfer for varying emissivity configurations were in excellent agreement with the analytical values. Finally, the conservation of radiative energy within the enclosure was confirmed to within 0.25%.

In addition to these validative comparisons, the results were also confirmed for physical consistencies whenever possible. For example, the temperature profiles were consistent with physical expectations while the total energy within the enclosure was conserved to within 0.2%. In addition, as discussed later, some of the results obtained here were consistent with those obtained by Paek and Runk [5]. Finally, the present model has been entirely incorporated into a larger, more recently updated work, where the predictions have been experimentally validated.

3.2. *Base system*

The base system consists of a preform with the experimentally measured shape, a furnace with a parabolic temperature distribution, and an axially variable heat transfer coefficient which varied from an absolute maximum value at the top to an absolute minimum value at the bottom with a cosinusoidal dependence. As noted earlier, these choices are explained in detail in Appendix A. The contours of the resulting streamfunction, vorticity, temperature and viscous dissipation function are shown in Fig. 3. In general, these contours were as expected, although the localization of the vorticity and viscous dissipation are noteworthy as it is a previously unknown phenomenon. As discussed in detail previously [10], these give rise to localized heating and possible material re-distribution.

Shown in Fig. 4 is the axial distribution of the heat flux, temperature and velocity, where the asterisks have been dropped for convenience. Shown in Fig. 4(a) is the heat flux incident on the preform, which starting at the top, decreased in the axial direction away from the radiant-balance iris. As the effect of the iris diminished, this flux increased in the direction of increasing furnace temperature, and attained a maximum value (near $z = 0.125$ m), prior to the location of maximum furnace temperature ($z = 0.137$ m). The resulting preform temperature distribution is shown in Fig. 4(b), where consistent with the requirement of continuous drawing, a monotonic behavior was found. That is, a continuous fiber requires the temperature to increase and decrease monotonically, otherwise the resulting uneven tension will cause fiber breakage. In addition, the dimensionless preform temperature attained a maximum value of 1.2 (2280 K) at the location of maximum heat flux. These are all very similar to the results found by Paek and Runk [5], and thus it is deduced that the present base configuration closely approximated physical reality. The corresponding temperature and velocity lags (defined to be the difference between the surface and center value divided by the center value) are also shown in Figs. 4(c) and (d), where, in Fig. 4(c), a very small velocity gradient was found. While it is unlikely that this would significantly alter the material distribution, it should be noted that this gradient could be more pronounced for materials with a stronger surface ten-

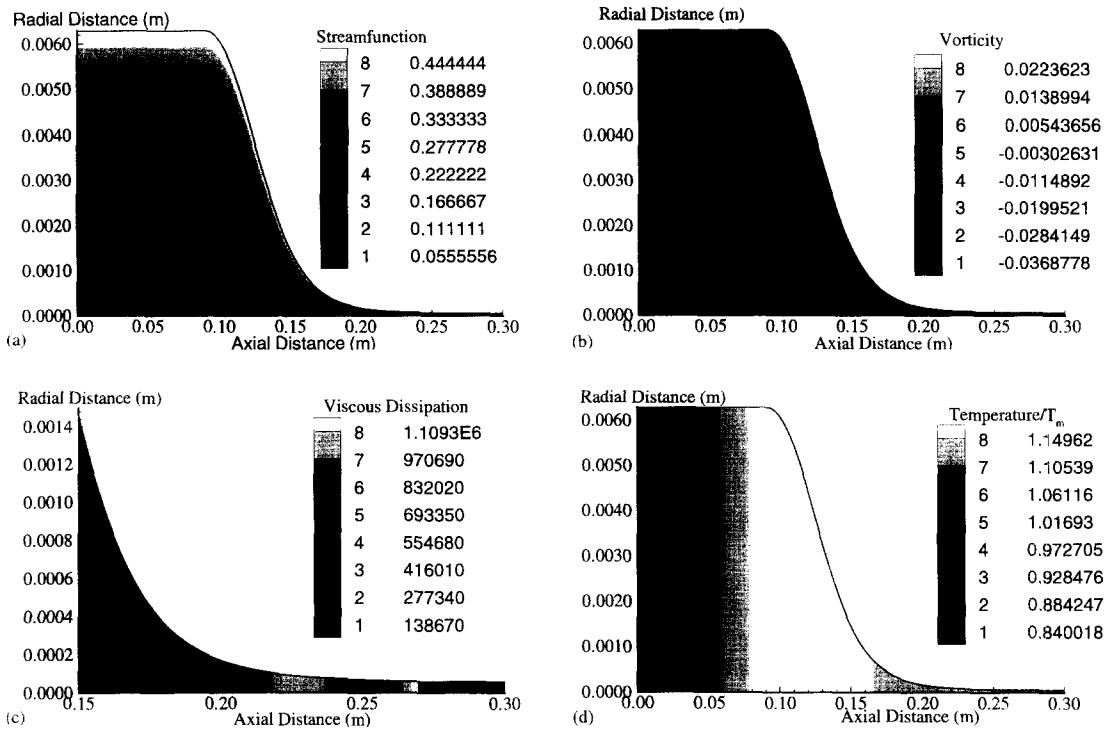

Fig. 3. Simulation results showing the contours of (a) streamfunction, (b) vorticity, (c) viscous dissipation function and (d) temperature (drawing speed = 300 cm s^{-1}, furnace set-temperature = 3000 K).

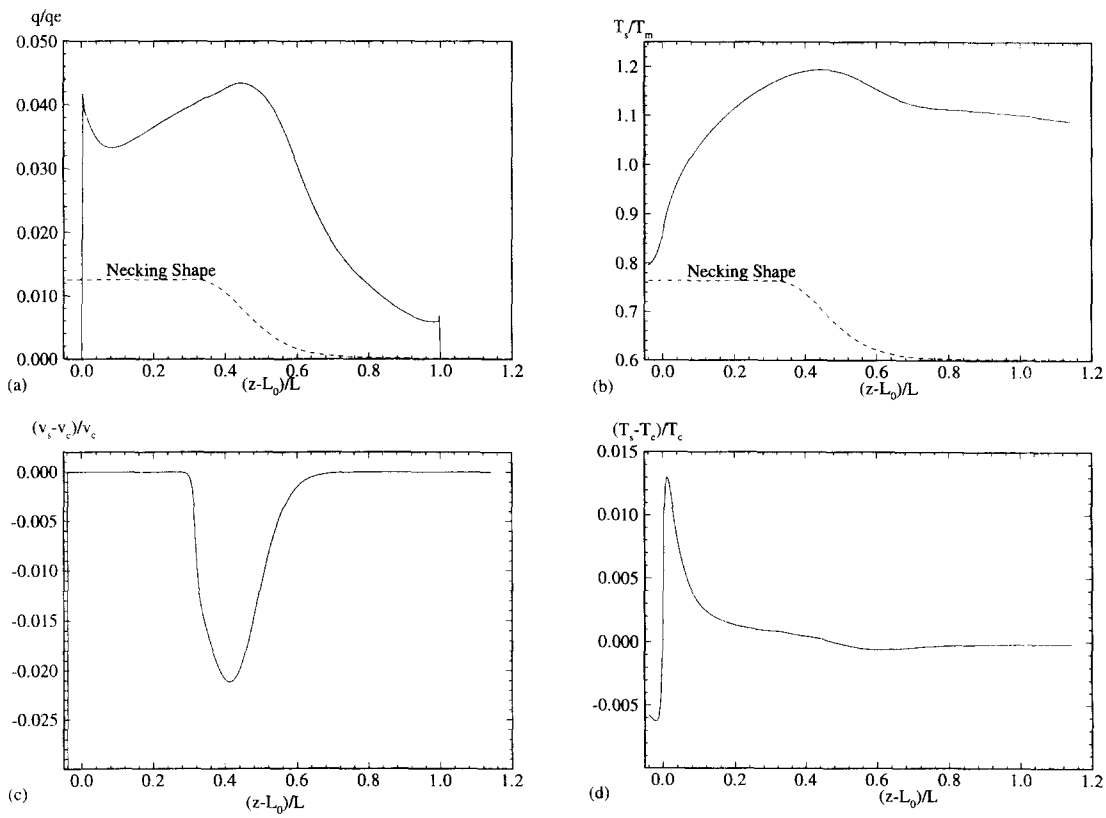

Fig. 4. Simulation results showing the axial profiles of the dimensionless (a) heat flux from the furnace, (b) surface temperature, (c) velocity lag and (d) temperature lag (drawing speed = 300 cm s^{-1}, furnace set-temperature = 300 K).

sion dependence, as may occur under different doping conditions. As for the temperature lag, Fig. 4(d) shows a considerably larger temperature gradient near the entrance of the furnace. This hints at the possibility of localized defects generation, which has been hypothesized to be related to temperature gradients [1].

3.3. *Neck shape*

The effect of varying the preform shape is considered. The interest here is to determine its impact on the overall solution. The two profiles considered were designated as case 1 and case 2, with case 1 representing the profile as measured by Paek and Runk [5]. Case 2 represents a half-period cosinusoidal shape with the same inlet and exit diameters as case 1. In Fig. 5(a) a comparison between the surface temperatures of case 1 and case 2 reveals that the assumption of a cosinusoidal variation resulted in a non-monotonic distribution, where it increased dramatically near the end of the neck-down region due to the previously mentioned localized viscous dissipation. This non-monotonic distribution violates the physical requirement of continuous drawing and is unrealistic. In addition, the variation in the necking shape also produced differences in the temperature and velocity lag profiles, as respectively shown in Figs. 5(b) and (c), where the difference in the velocity lag was much more significant. From these, it is evident that an accurate necking shape is of first-order importance in the current work. While this has never been previously shown, it is hardly surprising given the spectral dependence of the silica preform and the fact that the shape represents a tensile force balance which is coupled with the equilibrium of the transport.

3.4. *Thermal conditions*

It is also of interest to determine the effect of variations in the furnace temperature and heat transfer coefficient profiles. As mentioned earlier, this is motivated by the large number of researchers who tended to overlook the impact of an error in their assumptions of the convective heat transfer and the furnace temperature.

As noted in Appendix A, a parabolic temperature distribution has been assumed for the furnace, which is consistent with the deductions of Paek and Runk [5]. However, it is important to determine the effect of an error in this profile. Thus, three other distributions were used in this study. Case 1 designates the base configuration with the parabolic distribution, whereas case 2, case 3 and case 4 designate uniform distributions of 3000 K, 2800 K and 2600 K, respectively. Thus, this is also intended to verify the necessity of an axial variation in the furnace temperature, since most commercial furnaces can provide only one setting for the maximum temperature. The resulting surface temperatures on the preform are shown in Fig. 6(a). While it is not feasible to distinguish from this figure the appropriateness of the furnace temperature distribution, this figure clearly demonstrates the substantial impact of the furnace temperature. Thus, this shows, for the first time, the necessity of obtaining an accurate measurement of the furnace temperature. In addition, this also shows the errors committed by the previous researchers who tended to arbitrarily assume this temperature.

In an actual drawing furnace, inert gas is radially injected to yield aiding and opposing regions. This combined with the natural convection within gives rise to a fairly complex flow system. At the very least, the heat transfer coefficient, h, is expected to be axially variable, and, in general, increasing with increasing fiber speed. Yet, there has been very little effort to compute this dependence. In fact, it is not uncommon for researchers to assume a constant h value. Thus, it is of interest to determine the effect of neglecting this axial variation by comparing the results for the base system (case 1) with those for constant h values of 150 [W m^{-2}] (case 2), 300 [W m^{-2}] (case 3). This comparison is shown in Fig. 6(b) where again, except for the obvious non-monotonic behavior of case 3, it is quite difficult to identify the appropriate heat transfer coefficient profile. However, it is clear that while case 3 is unacceptable, case 1 and case 2 produced significant differences in the fiber temperature. Not only will this difference affect the later coating stage, but it is also expected to shift the above-mentioned equilibrium and thus alter the necking shape.

3.5. *Approximations*

Solving the full sets of momentum and energy equation is computationally intensive. Therefore, it is desirable to obtain an approximation to the full equations. The two possibilities evaluated were designated as the constant properties and zero-vorticity approximations. The first involves calculating the full equations where all the properties (viscosity, conductivity and specific heat) were evaluated at one characteristic temperature, while the second is to assume that the momentum and thermal transport do not significantly affect each other. This is referred to as the zero-vorticity approximation, since one could essentially calculate the velocity from the streamfunction equation with the vorticity set to zero and then use the resulting velocity to find the temperature distributions.

The constant properties assumption is based on the assumption that there may exist some characteristic temperature at which the properties could be evaluated to allow for a quick approximate solution. These temperatures were chosen to be 1.1, 1.2 and 1.3 multiples of T_m, and are respectively designated as case 1, case 2 and case 3. Their results are contrasted with those of the base system (case 4), and are presented in Fig. 7. As shown in Fig. 7(a), there exist minor differences in the resulting surface temperatures, although the difference seemed to be more pronounced in the temperature lag profiles shown in Fig. 7(b), where the variations of the thermal diffusivity played a major role. While this approximation does not properly capture the temperature gradient, it

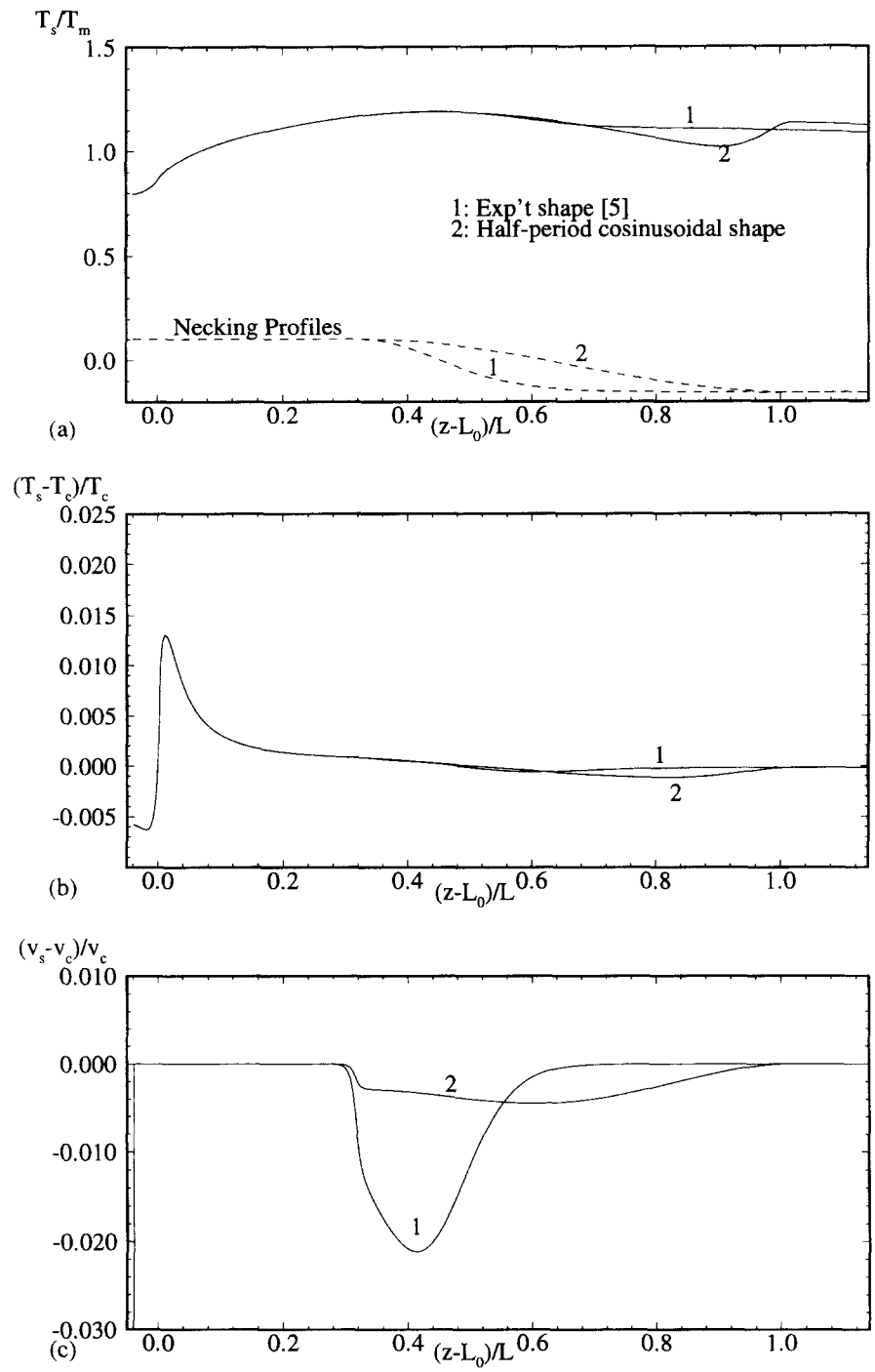

Fig. 5. Results showing the effect of varying the preform's shape on the dimensionless (a) surface temperature, (b) temperature lag and (c) velocity lag.

adequately captures the velocity gradient, as shown in Fig. 7(c) where the velocity lag profiles were nearly identical.

In the second approximation, the goal is to reduce the computational time by uncoupling the momentum and energy equations. From Fig. 3(d) it was observed that the heat transfer within most of the medium is dominated by conduction, except in the fiber portion where there exists very little radial flow anyway. That is, while the local temperature is affected by the bulk motion, it may be less sensitive to the particular velocity distribution. Consequently, the velocity can be determined from a single iteration of the stream-function equation, with the vorticity set to zero. With this velocity, the energy equation can then be solved until convergence, with the associated computational

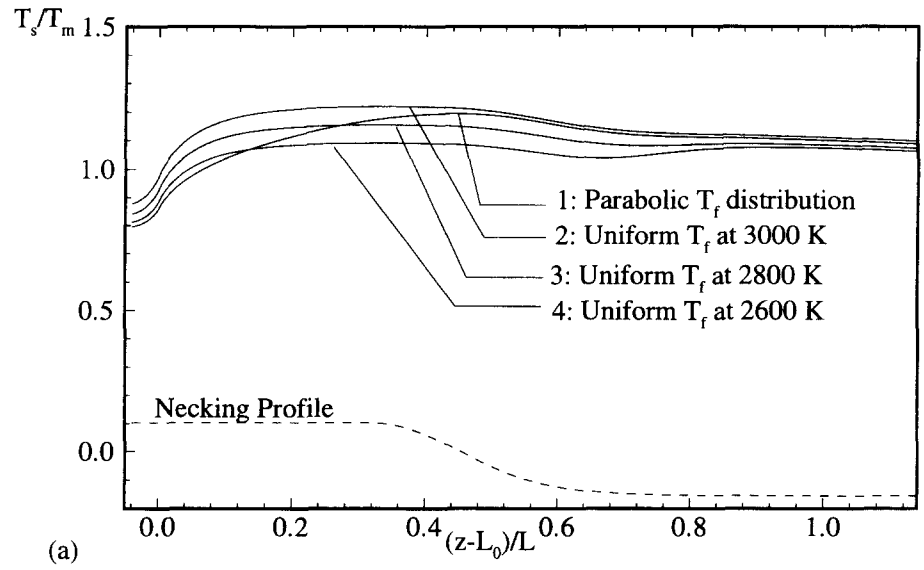

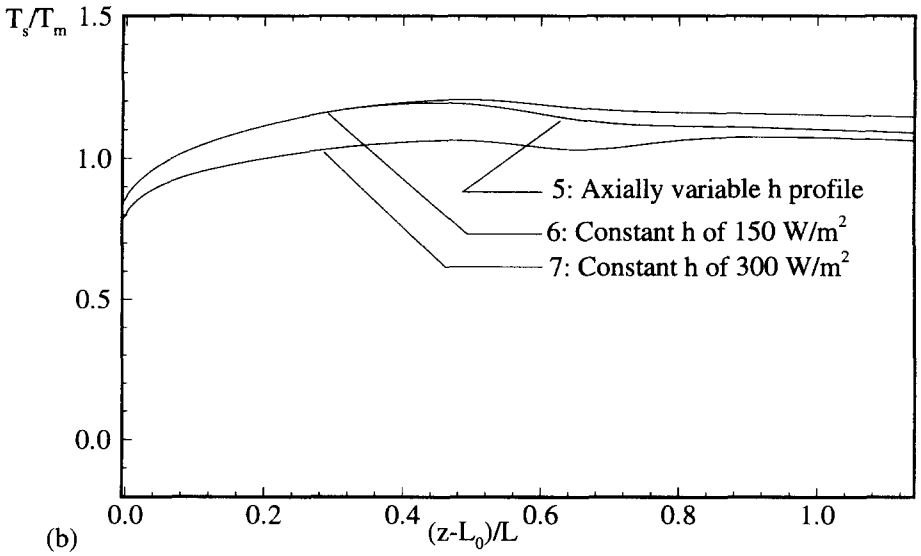

Fig. 6. Results illustrating the effect of varying (a) the furnace temperature distribution and (b) the heat transfer coefficient profiles on the dimensionless surface temperature of the preform.

time reduced to 1/3. The results are presented in Fig. 8, where substantial similarities exist not only in the surface temperature but also in the temperature lag profiles. It is interesting to note that these similarities implied proper computation of the viscous dissipation. Since this approximation assumed zero vorticity everywhere, this, in turn, implied the viscous dissipation to be unaffected by the vorticity. While this approximation had minimal impact on the temperature distribution, it did, as expected, significantly affect the velocity distribution, as shown in Fig. 8(c). In fact, the assumption of zero vorticity caused inconsistency with the uniform inlet condition, as shown, in Fig. 8(c), by the jump in the velocity near the entrance.

4. CONCLUSIONS

The furnace drawing of 1.25 cm diameter fused silica was simulated. The drawing speed was 300 cm s^{-1} and the associated drawing conditions were consistent with those previously measured. Heat flux, velocity and temperature distributions were obtained. The computed results were consistent with physical expectations and previously published results. In addition, the results showed a previously unknown

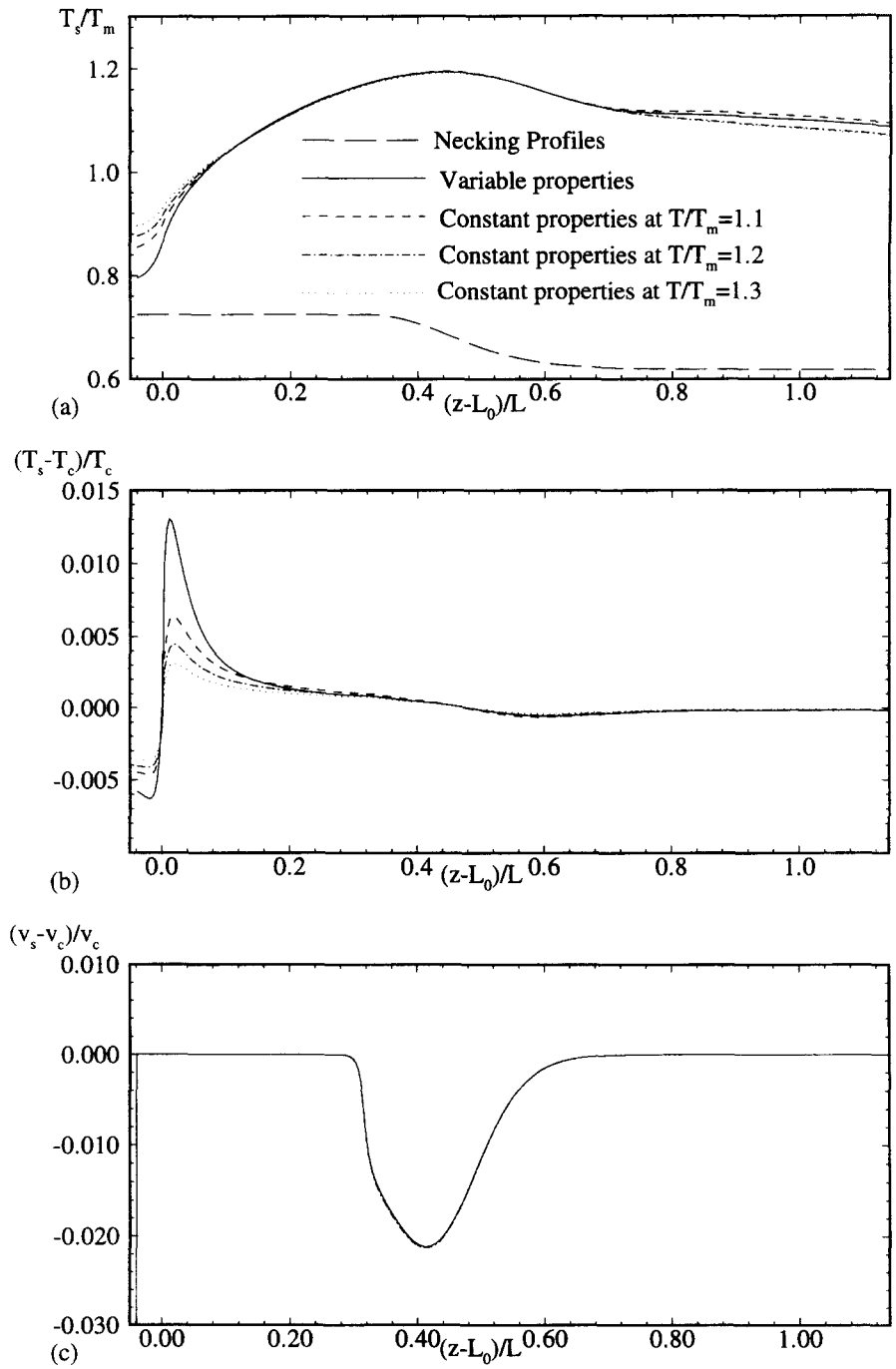

Fig. 7. Comparisons of the dimensionless (a) surface temperature, (b) temperature lag and (c) velocity lag computed through the constant properties approximation.

localization of the vorticity and viscous dissipation, the latter of which tended to produce significant differences in the fiber temperature. The results also confirmed, for the first time, the existence of temperature and velocity gradients. As expected, the largest temperature gradient existed in the region immediately after entering the furnace. As there may be a relation between this gradient and fiber defects, one potential solution is to change the furnace configuration (i.e. furnace length and temperature distribution) so as to minimize the resulting gradient. The velocity gradient is also of concern as it could give rise to material re-distribution. Although the computed velocity gradient is fairly small, it should be noted that this could be altered under different doping conditions.

The effects of variations in the necking shape, the heat transfer coefficient and the furnace temperature

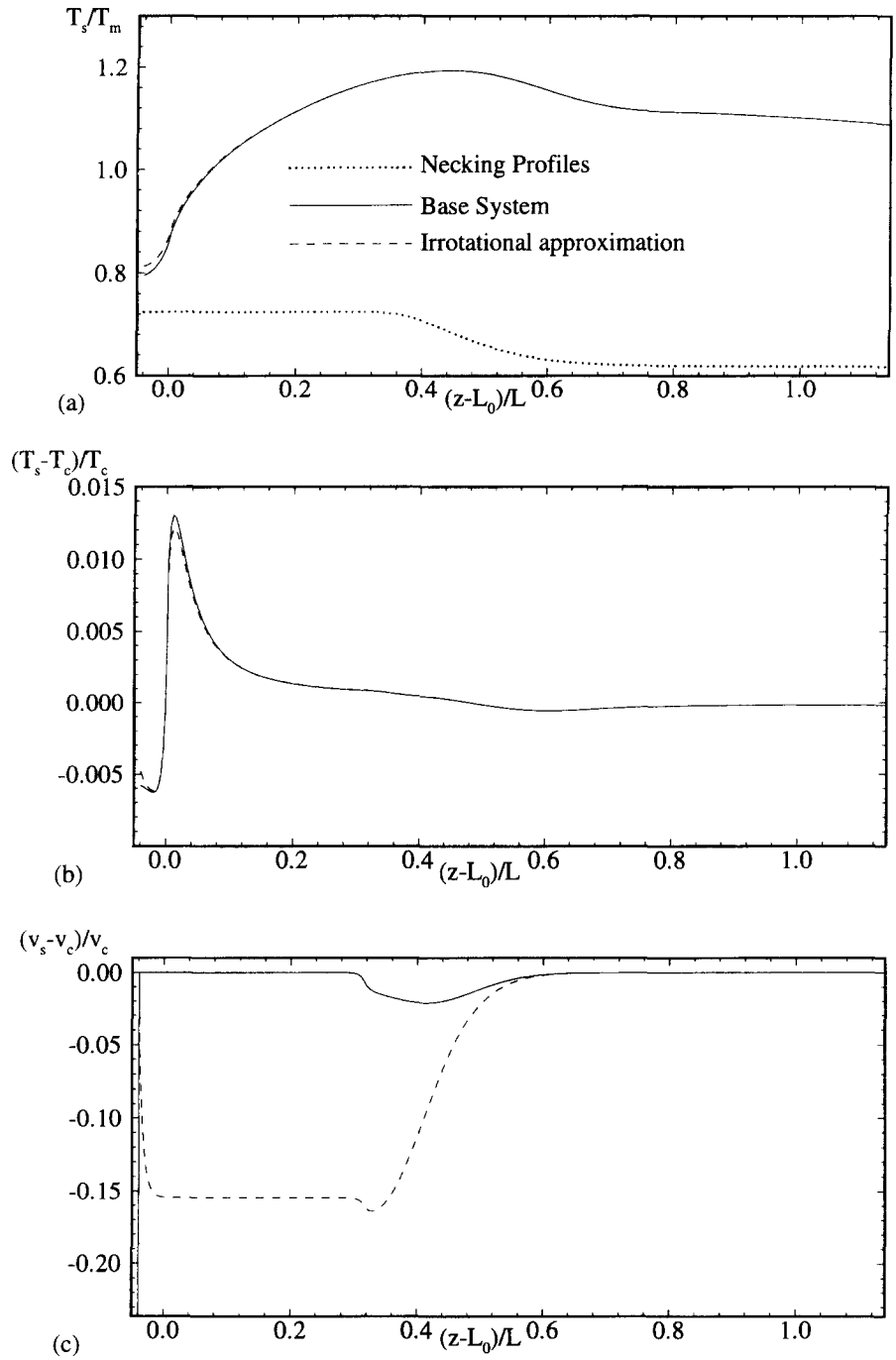

Fig. 8. Comparisons of the dimensionless (a) surface temperature, (b) temperature lag and (c) velocity lag computed through the zero-vorticity approximation.

profiles were also studied. As mentioned earlier, this is motivated by the fact that many of these factors are largely unknown. The results clearly showed their significant impact on the overall solution. Of these three factors, the implication of the necking shape dependency is smaller as it can often be determined experimentally, although this would not be viable for studies involving previously unknown drawing conditions. Under this latter scenario, the necking shape must necessarily be generated as part of the solution. The implications of the heat transfer coefficient and furnace temperature dependency are much more substantial as their values are still very much unknown. Thus, this also brings into question the many previous studies which tended to arbitrarily assume their functional forms. Clearly, much more accurate information on the heat transfer coefficient and the furnace temperature profiles is critically required.

Approximate solutions have also been obtained. Two schemes were attempted: the first assumed constant properties evaluated at some characteristic temperature, while the second assumed zero vorticity everywhere. Results showed the first scheme to be of limited value as it cannot properly account for the temperature gradients in the radial direction. The second scheme showed much more potential, as it properly computed both the surface temperature as well as the temperature gradients. However, it did not properly compute the velocity lag profiles, and, as such, its usefulness is limited to applications where the velocity distribution is of minimal interest.

Acknowledgements—The authors wish to acknowledge the assistance of Prof. U. C. Paek, the financial support from the National Science Foundation under grant DDM-92-13458, the Hong Kong Telecom Institute of Information Technology under grant HKTIIT94/95.EG02 and the computational resource provided by the Pittsburgh Supercomputer Center under grant CTS930050P.

REFERENCES

1. Hanafusa, H., Hibino, Y. and Yamamoto, F., Formation mechanism of drawing induced e' centers in silica optical fibers. *Journal of Applied Physics*, 1985, **58,** 1356.
2. Paek, U. C. and Kurkjian, C. R., Calculation of cooling rate and induced stresses in drawing of optical fibers. *Journal of the American Ceramic Society*, 1975, **58,** 330–335.
3. Fleming, J. D., Fused silica manual, Final Report for The U.S. Atomic Energy Commission, Oak Ridge, Tennessee, Project no. B-153 (1964).
4. Lee, S. H.-K., Numerical investigation on the neck-down region of a furnace-drawn optical fiber. Ph.D. Dissertation, Rutgers University, New Brunswick, NJ, 1993.
5. Paek, U. C. and Runk, R. B., Physical behavior of the neck-down region during furnace drawing of silica fibers. *Journal of Applied Physics*, 1978, **49,** 4417–4422.
6. Sayles, R., A finite element analysis of the upper jet region of a fiber drawing flow field. Ph.D. thesis, Brown University, Providence, RI, 1982.
7. Myers, M. R., A model for unsteady analysis of preform drawing. *AIChE Journal*, 1989, **35,** 592–602.
8. Lee, S. H.-K. and Jaluria, Y., The effects of streamwise convergence in radius on the laminar forced convection in axisymmetric ducts. *Numerical Heat Transfer, Part A*, 1995, **28,** 19–38.
9. Lee, S. H.-K. and Jaluria, Y., The effects of geometry and temperature variations on the radiative transport during optical fiber drawing. *Journal of Materials Processing and Manufacturing Science*, 1995, **3,** 317–331.
10. Lee, S. H.-K. and Jaluria, Y., Effects of variable properties and viscous dissipation during optical fiber drawing. *Journal of Heat Transfer*, 1996, **118,** 350–358.
11. Glicksman, L. R., The cooling of optical fibres. *Glass Technology*, 1968, **9,** 131.
12. Landau, H. G., Heat conduction in a melting solid. *Applied Mathematics Quarterly*, 1950, **8,** 81–94.
13. Levich, V. G. and Krylov, V. S., Surface-tension driven phenomena. *Annual Review of Fluid Mechanics*, 1969, **1,** 293–316.
14. Patankar, S. V., *Numerical Heat Transfer and Fluid Flow*. Hemisphere, New York, 1980.
15. Jaluria, Y. and Torrance, K. E., *Computational Heat Transfer*. Hemisphere, New York, 1986.
16. Krishnan, K. N. and Sastri, V. M. K., Numerical solution of thermal entry length problem with variable viscosities and viscous dissipation. *Wärme und Stoffübertragung*, 1978, **11,** 73–79.
17. Lawal, A. and Mujumdar, A. S., Viscous dissipation effects on thermal entrance heat transfer to power-law fluids in arbitrary cross-sectional ducts. *The Chemical Engineering Journal*, 1989, **41,** 57–66.
18. Lin, T. F., Hawks, K. H. and Leidenfrost, W., Analysis of viscous dissipation effect on thermal entrance heat transfer in laminar pipe flows with convective boundary conditions, *Wärme und Stoffübertragung*, 1983, **17,** 97–105.
19. Ou, J. W. and Cheng, K. C., Viscous dissipation effects on thermal entrance region heat transfer in pipes with uniform wall heat flux. *Applied Scientific Research*, 1973, **28,** 289–301.
20. Yang, K. T., Laminar forced convection of liquids in tubes with variable viscosity. *Journal of Heat Transfer*, 1962, **94,** 353–362.
21. Garg, V. K. and Maji, P. K., Flow through a converging–diverging tube with constant wall enthalpy. *Numerical Heat Transfer*, 1987, **12,** 285–305.
22. Vaskopulos, T., Forced fiber cooling. Ph.D. dissertation, Rutgers University, New Brunswick, NJ, 1994.
23. Javeri, V., Simultaneous development of the laminar velocity and temperature fields in a circular duct for the temperature boundary condition of the third kind. *International Journal of Heat and Mass Transfer*, 1976, **19,** 943–949.
24. Mohanty, A. K. and Asthana, S. B. L., Laminar flow in the entrance region of a smooth pipe. *Journal of Fluid Mechanics*, 1978, **90,** 433–447.
25. Siegel, R. and Howell, J. R., *Thermal Radiation Heat Transfer*. McGraw-Hill, New York, 1981.
26. Uhlmann, D. R. and Kreidl, N. J., *Glass Science and Technology*. Academic Press, New York, 1984.

APPENDIX A: GEOMETRICAL CONFIGURATION

The length of the preform, L_f, was taken to be 0.3 m with an exit velocity, V_e, of 3 m s^{-1}. The top and bottom of the furnace were assumed to be shielded by irises, and the preform was offset from the top of the furnace with a length, L_0, of 1 cm. The neck profile was taken from the measurement of Paek and Runk [5], as given in equation (A1a). This profile was also varied in order to determine its impact on the overall solution, as given below in equation (A1b).

$$\text{For } z < z_1 = 0.09 \text{ m}: \quad R = R_i = 0.006288 \text{ m}$$
$$\text{For } z > z_2 = 0.27 \text{ m}: \quad R = R_e = 0.000059 \text{ m} \tag{A1a}$$

For $z_1 \leqslant z \leqslant z_2$:

$$\begin{aligned}\text{Log}_{10}R = {} & -6.66531\times10^5(z-(z_1-0.02))^8 \\ & +1.5152\times10^6(z-(z_1-0.02))^7 \\ & -6.20906\times10^5(z-(z_1-0.02))^6+1.56512\times10^4 \\ & \times(z-(z_1-0.02))^5+3.0826\times10^4(z-(z_1-0.02))^4 \\ & -4.71803\times10^3(z-(z_1-0.02))^3+78.84(z-(z_1-0.02))^2 \\ & +1.57224(z-(z_1-0.02))-2.231642\end{aligned}$$

Cosinusoidal shape:

$$\text{For } z < z_1 = 0.09 \text{ m}: \quad R = R_i = 0.006288 \text{ m}$$
$$\text{For } z > z_2 = 0.27 \text{ m}: \quad R = R_e = 0.000059 \text{ m}$$

For $z_1 \leqslant z \leqslant z_2$:

$$R = \frac{R_i+R_e}{2}+\frac{R_i-R_e}{2}\cos\pi\left(\frac{z-z_1}{z_2-z_1}\right). \tag{A1b}$$

The preform is heated by a furnace whose radius, R_0, is 1.9 cm and whose length, L, is 25.4 cm. The typical operating temperature of this furnace is around 2300 K [5], and its temperature profile is symmetrical length-wise with a maximum value at the center. This maximum temperature is also the furnace set-temperature as most furnaces have a pyrometer focused at their center. A parabolic temperature profile was assumed in this study with minimum temperatures of 2300 K at the top and bottom of the furnace and a maximum center temperature. The value of this maximum temperature is not known, and was determined here to be 3000 K by successively decreasing its value until, at the next lower temperature, the surface temperature of the preform exhibited an unrealistic profile. Here an unrealistic profile is taken to be one with multiple local maxima, since this would give rise to uneven tension and thus cause fiber breakage.

In addition to the radiative exchange with the furnace, the preform also convects heat to the surrounding gas at 1373 K. Similar to the analyses of Paek and Runk [5] and Glicksman [11], a heat transfer coefficient, which varies axially, was assumed for this convective exchange. Taking the minimum and maximum values from Paek and Runk [5], a half-period cosinusoidal variation was assumed, as given below in equation (A2).

$$\text{For } z < z_1 = 0.09 \text{ m}: \quad h = h_i = 150 \text{ W m}^{-2}$$

$$\text{For } z > z_2 = 0.27 \text{ m}: \quad h = h_e = 300 \text{ W m}^{-2} \tag{A2}$$

$$\text{For } z_1 \leqslant z \leqslant z_2:$$

$$h = \frac{h_i + h_e}{2} + \frac{|h_i - h_e|}{2} \times \cos \pi \left(\frac{z - z_1}{z_2 - z_1} + \frac{1}{2} - \frac{|h_i - h_e|}{2(h_i - h_e)} \right).$$

APPENDIX B: PROPERTY VARIATIONS

To simulate realistic fiber drawing conditions, the hemispherical, total, emissivity of the furnace was taken to be 0.75 [5]. Also, following Myers' approach [7], the hemispherical, spectral, emissivity values for fused silica from Sayles' study [6] were used for the fiber. In addition to the radiative properties, the thermal conductivity, surface tension, specific heat and viscosity were also taken to be temperature dependent. These values were all taken from either Fleming's [3] or Myers' studies [7] and whenever possible, cross-checked against each other. The thermal conductivity was obtained from curve-fitting the data [3] with a third-order polynomial, as given below in equation (A3a).

$$\text{For } 310.78 \text{ K} \leqslant T \leqslant 1921.89 \text{ K}$$

$$k_c(T) = -1.6874325 \times 10^{-11} \left(\frac{9T}{5} - 459.4 \right)^3 + 4.7386566 \times 10^{-9} \left(\frac{9T}{5} - 459.4 \right)^2 + 4.3111737 \times 10^{-4} \left(\frac{9T}{5} - 459.4 \right) + 1.3424434$$

$$\text{For } T < 310.78 \text{ K}: \quad k_c = k_c(310.78)$$

$$\text{For } T > 1921.89 \text{ K}: \quad k_c = k_c(1921.89). \tag{A3a}$$

This conductivity was combined with a radiative component obtained by using Rosseland's assumption to approximate the radiative transport within the necking preform. This approach, taken from Myers' report [7], assumed an optically thick medium, and its applicability may not be clear. However, since this is outside the scope of this work, it has been adapted here for convenience, as given in equation (A3b).

$$k_r = \frac{16 n^2 \sigma T^3}{3a}$$

$$= \frac{16(1.42)^2 5.729 \times 10^{-8}}{3} = 1.5402607 \times 10^{-9} T^3. \tag{A3b}$$

The temperature dependence of the surface tension and specific heat were also obtained by curve-fitting against Fleming's data [3]. These are given in equations (A4) and (A5) as:

$$\text{For } T < T_m, \quad \xi = 0.17315$$

$$\text{For } T \geqslant T_m, \quad \xi = 3.375 \times 10^{-5} T + 0.10902625 \tag{A4}$$

For 310.78 K $\leqslant T \leqslant$ 1699.67 K

$$c_p(T) = -1.9202379 \times 10^{-11} \left(\frac{9T}{5} - 459.4 \right)^4 + 8.9608033 \times 10^{-8} \left(\frac{9T}{5} - 459.4 \right)^3 - 2.0008399 \times 10^{-4} \left(\frac{9T}{5} - 459.4 \right)^2 + 0.59235423 \left(\frac{9T}{5} - 459.4 \right) + 6.2175046 \times 10^2$$

$$\text{For } T < 310.78 \text{ K}: \quad c_p = c_p(310.78)$$

$$\text{For } T > 1699.67 \text{ K}: \quad c_p = c_p(1699.67). \tag{A5}$$

Finally, equation (A6) gives the exponential dependence of the kinematic viscosity on the temperature. This was adapted from Myers' data [7] and also verified with Fleming's data [3].

$$\nu(T) = 4545.45 \exp \left[32 \left(\frac{T_m}{T} - 1 \right) \right]. \tag{A6}$$

Equation (A6) assumes that the entire fused silica behaves as a Newtonian fluid with the viscosity varying exponentially with the temperature. This is consistent with the non-crystalline structure of glass, where the apparently solid portion is a fluid with a large viscosity. This assumption essentially ignores any viscoelastic or non-Newtonian behavior of the silica, since in general, very little is known about the behavior of fused silica under this flow configuration. However, it is clear that any viscoelastic effect will be minimal as the drawing tension is only of the order of 0.1 N. In addition, it is widely accepted that at a low rate of deformation, glass behaves as a Newtonian fluid [26]. While in the current system the deformation may be high, its rate may not be high as the feeding rate is low. Also, while the final drawing velocity is large, most of the deformation occurs under a relatively low velocity condition.